

Pres. 1st Workshop on Electronics for
LHC Experiments, Lisbon, Portugal
10-15 September 1995. To appear in:
Proceedings of this Workshop.

BNL -62328

ELECTRONICS FOR CALORIMETRY - AN OVERVIEW OF REQUIREMENTS*

V. Radeka

**Brookhaven National Laboratory
Upton, NY 11973-5000**

October, 1995

*This research was supported by the U. S. Department of Energy:

MASTER

DISTRIBUTION OF THIS DOCUMENT IS UNLIMITED

DISCLAIMER

**Portions of this document may be illegible
in electronic image products. Images are
produced from the best available original
document.**

Electronics for Calorimetry - an Overview of Requirements*

V. Radeka

Brookhaven National Laboratory, Upton, NY 11973-5000

1. INTRODUCTION

Calorimetry in large detectors at LHC poses some requirements on readout electronics which are quite different than for central tracking and muon tracking. The main distinction is, a) in the large dynamic range of the energies to be measured; and b) uniformity of response and accuracy of calibration over the whole detector. As in all other functions of the detector, low noise is essential. High luminosity results in pileup effects, which are present in every measurement, and in high radiation for front and forward parts of the calorimeter. Power dissipation and cooling is a concern as in any other detector component, in some respects only more so, since all the elements of the signal processing chain require more power due to the large dynamic range, speed of response, high precision and low noise required.

The key requirements on the calorimetry readout electronics are briefly discussed here, with an emphasis on the dynamic range.

While there are quite significant differences in the principles and technology among the crystals, tiles with fibers and liquid ionization, the signal is finally reduced to a charge measurement from a capacitive source in all three cases, and the signal processing chain becomes remarkably identical.

2. SUMMARY OF KEY REQUIREMENTS

In this section, some key requirements arising from physics considerations are listed:

Physics requirements on calorimetry:

Energy Resolution:

EM: $< 10\%/\sqrt{E}$; constant term $< 0.7\%$

HAD: $< 50\%/\sqrt{E}$; constant term $< 3\%$

FORWARD: $< 100\%/\sqrt{E}$; constant term $< 10\%$

Electron/hadron Resp.: < 1.1 (direct or by weighting)
(e.g., for quark compositeness signal)

Photon Identification:

High granularity for shower isolation
Preshower for additional π^0 rejection ($\sim 3x$)

EM Shower Direction Measurement: < 50 mrad/ \sqrt{E}
2-4 longitudinal divisions (including preshower)

Hermeticity:

Depth: EM $\sim 25 X_0$; HAD $\sim 11\lambda$

η Coverage: EM fine granularity to ± 2.5 ; coarse to ± 3.2

η Coverage: HAD with Forward Calorimeter to ± 5

Radiation Environment:

Integrated Dose:

EM Barrel $\sim 5 \times 10^4$ rad/year

EM Endcap $\sim 2 \times 10^4 - 5 \times 10^6$ rad/year

Neutron Flux:

EM Barrel $\sim 10^{13}$ neutrons/cm².year

EM Endcap $\sim 10^{14}$ neutrons/cm².year

Number of Channels: $> 2 \times 10^5$

Including EM + HAD + Integrated Preshower

(can be a few 100k channels more for non integrated preshower)

Dynamic Range: 16 - 17 bits

Lower limit from electronic noise: $\sim 25-35$

MeV/channel or tower

Upper limit from $Z' \rightarrow ee$ and $W' \rightarrow ev$: ~ 3 TeV

Hadr. : from muons to ~ 1 TeV

Speed and Pileup:

Timing (associate events and bunch crossings): $\sigma_t \sim 1-2$ nsec

Shaping time: EM ~ 20 nsec; HAD $< 20-50$ nsec

Lepton isolation, timing for E $\sim 0.3 - 1$ GeV

Systematics:

(Calibration + Digitization + Uniformity + Stability)
 $< 1\%$

$\sim 0.2 - 0.3\%$

*This research was supported by the U.S. Department of Energy: Contract No. DE-AC02-76CH00016.

dic

3. SIGNALS, SOURCES, NOISE AND PILEUP

There is quite a diversity in the calorimetry techniques in the two proposed large experiments ATLAS and CMS. From the point of view of sampling and measurement of the energy deposited in the calorimeter, the calorimeter techniques fall into two broad categories, based on the effects of particle interaction with the sensing medium to be observed: scintillation and ionization. Scintillation based devices are coupled to photodetectors. The properties of the signal source are then determined by the photodetector and by the electrode configuration in an ionization calorimeter. The techniques employed in CMS and ATLAS are summarized in Table I. Included, also, for orientation are the typical values of electrode capacitance, noise and expected signal. Typical signal waveforms are illustrated in Fig. 1. The electronic noise is assumed to be entirely due to the series noise in the input transistor. The parallel noise from any source can be (and should be) made negligible at the short shaping times (20 to 50 ns) required in calorimetry at the LHC luminosities. For approximate estimation of the series noise, the following expression may be used,

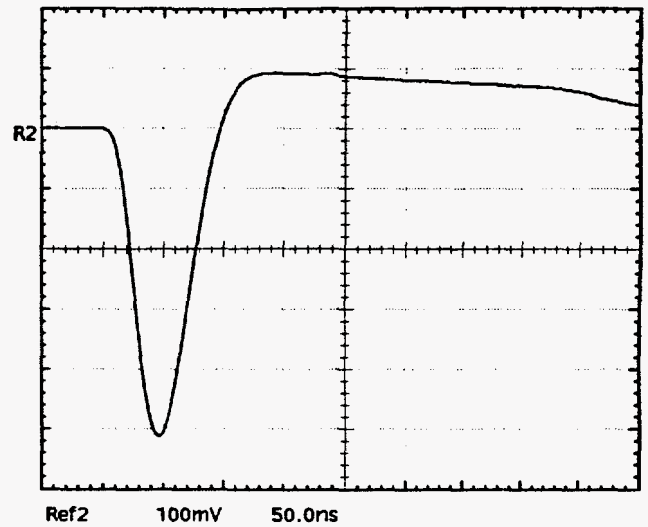
$$ENC = e_n \cdot C_{in}/t_m^{1/2} \quad (1)$$

where e_n is the equivalent series noise voltage spectral density, C_{in} is the total input capacitance ($C_{det} + C_A$, detector plus amplifier), and t_m is the zero-to-peak time for a symmetrical triangular unipolar weighting function approximating the impulse response of a real system. (For detailed noise analysis, see References 1,2,3, where also further references are given.) t_m is also an effective integration time. In Table I, the value of 25 ns was assumed in all cases. It may be somewhat shorter (~20 ns), but not by much, considering the signals in Fig. 1, charge transfer times, and also the requirement to realize linear shaping amplifiers and sampling circuits. In hadron calorimeters, particularly in the back sections (compartments), t_m may be (and may have to be) longer (~ 50 nsec) to assure sufficient charge (light) collection and signal-to-noise ratio. In Table I, it was assumed that the amplifier input transistor would be chosen in size (width) to correspond to the detector capacitance (if not to match it exactly for minimum noise or at constant operating current). Thus at the lower end of the capacitance scale (< 100 pF), a transistor with $e_n = 1 \text{ nV/Hz}^{1/2}$ and $C_A = 10\text{-}20 \text{ pF}$ was assumed. At the high end for LAr, a GaAs transistor, with $e_n = 0.3 \text{ nV/Hz}^{1/2}$ and $C_A = 150 \text{ pF}$ at 90°K was assumed⁴.

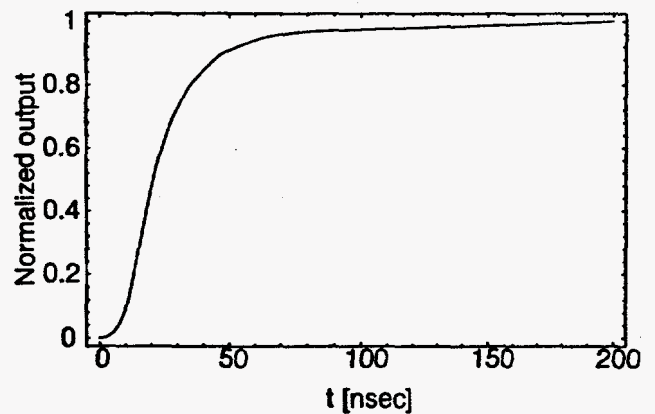
The following specific comments apply to different techniques:

Liquid Ionization Calorimetry. In the electromagnetic calorimeter with accordion electrodes, with liquid argon and a sampling fraction of ~ 22%, the ionization produced is ~ 6×10^6 electrons/GeV. The induced charge in $t_m = 25 \text{ ns}$ is Q_s

a: Liquid Argon signal after shaping



b: Charge vs. time for a tile calorimeter



c: Normalized current and charge for a crystal

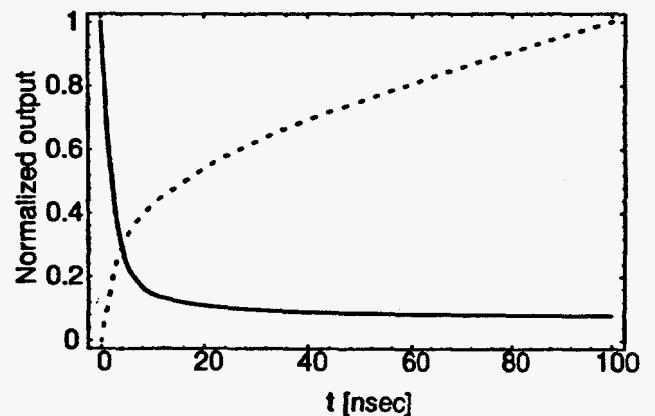
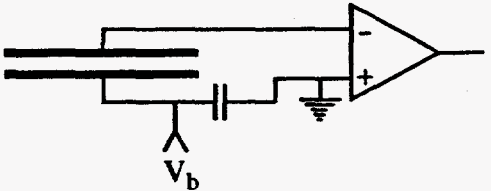
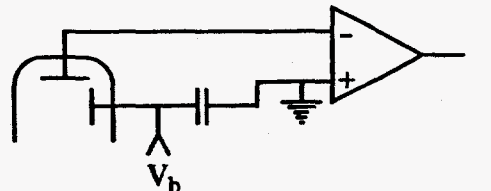
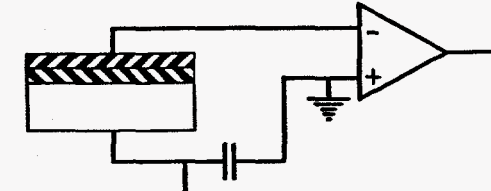
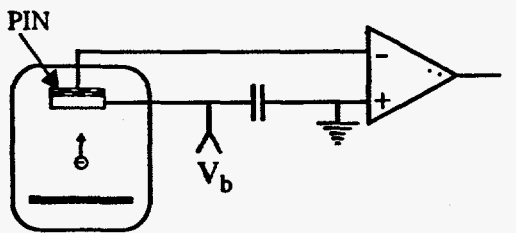


Fig. 1. Signal waveforms:

- a) LAr after shaping, $t_m = 25 \text{ ns}$, $t_p \approx 45 \text{ ns}$ (measured);
- b) tile calorimeter;
- c) PbWO_4 crystal

Table I: Readout Techniques for Calorimeters

	<u>CMS</u>	<u>ATLAS</u>		
<u>Presampler</u>	Silicon	LAr		
<u>EM</u>	Crystal	LAr		
<u>Hadronic Barrel</u>	Tile Cal.	Tile Cal.		
<u>Hadronic Endcap</u>	Tile Cal.	LAr + Tile Cal.		
<u>Forward</u>	Quartz Fiber	LAr		
		C_{det} [pF]	ENC [rms e] for $t_m \sim 25$ ns	Signal [e/GeV] in $t_m \sim 25$ ns
<u>LAr</u> (Liquid Argon)		$\sim 300-3000$	$\sim 6 \times 10^3 - 4 \times 10^4$	$\sim 4 \times 10^5$
<u>PM</u> (Photomultiplier)		~ 20	$\sim 1.6 \times 10^3$	$\sim 50 \times G_{PM}$
<u>APD</u> (Avalanche Photodiode)		$\sim 50-100$	$\sim 3 \times 10^3$	$\sim 3 \times 10^3 \times G_{APD}$
<u>HPM</u> (Hybrid Photo-multiplier)		$\sim 30-300$	$\sim 2-8 \times 10^3$	$\sim 50 \times G_{HPM}$

$\approx 4 \times 10^5$ electrons/GeV ≈ 0.06 picocoulombs/GeV. The maximum induced signal for 2 TeV, deposited in a single section (channel), is then ≈ 120 picocoulombs. The peak current is $I_m \approx 5$ mA, for a typical 2 mm interelectrode spacing and an electron drift time of ≈ 400 nsec. Due to the large amount of charge, the fluctuations in the signal waveform are negligible.

Scintillation tile and wavelength shifter fiber calorimetry. ("Tile cal"). The signal produced in a sampling calorimeter, with wavelength shifting fibers, is relatively small and some gain is required in the photodetector to overcome the amplifier noise. The exact value for the signal depends on many design parameters and scintillator properties. The value of 50 photoelectrons/GeV, from a vacuum photocathode, is assumed here to obtain an estimate for the gain required. Photodetectors coupled to fibers will be segmented into small electrodes, and the capacitance (with connections) will be low. Taking a value for the noise of 0.25 fc, and the extreme dynamic range of 10^5 , the maximum charge from the photodetector would be 25 pc $\approx 1.5 \times 10^8 e$. Assuming an upper limit for the energy from a jet deposited in a single compartment of ~ 3 TeV, the charge from the photocathode would be $\sim 1.5 \times 10^5 e$, requiring a gain of $\approx 10^3$. To determine an exact dynamic range, the information on the number of photoelectrons for a muon in one compartment is needed. (The dynamic range is likely to be less than 10^5 .) A gain of $\sim 10^3$ is within reach for hybrid photomultiplier devices, (known also as silicon intensified targets), and for secondary emission multipliers, which have to operate in a magnetic field.

The pulse shaping (integration time) may have to be longer than 25 ns, since ~ 45 ns is needed to observe 90% of the light charge).

Scintillator Crystal Calorimetry. The crystal under study for EM calorimetry in CMS is lead tungstate ($PbWO_4$). The optimization of the photoelectron yield and the photodetector is in the process, and an estimate of the required gain is limited by the information available now. Since a crystal is a homogeneous total absorption calorimeter, the light output will be higher than in a sampling calorimeter, and only a relatively low gain will be required. Due to the need to operate in a strong magnetic field, avalanche photodiodes are being considered. Optimization of the photoelectron yield, with respect to the diode capacitance, and diode as a particle detector, involves many variables. It is clearly of interest to keep the required avalanche gain as low as possible in order to minimize the excess noise and have better gain stability. The photoelectron yield given in Table I is, at best, tentative. In this example, the yield per GeV is about equal to the electronic noise in rms electrons expected. To reduce the electronic noise to ~ 30 MeV/tower, an avalanche gain of ~ 30 would be required. For an energy deposition of 2 TeV in a single tower, the output charge will be $\sim 2 \times 10^8 e \sim 32$

picocoulombs. The dynamic range in this case would be $\sim 7 \times 10^4$.

The time response of crystal scintillators has usually more than one component. The response of some recently measured lead tungstate crystals can be best fitted by a three component expression⁵,

$$y = A_1 \exp(-t/\tau_1) + A_2 \exp(-t/\tau_2) + A_3 \exp(-t/\tau_3) \quad (2)$$

$A_1 = 10^3$	$A_2 = 135$	$A_3 = 49$
$\tau_1 = 2.1$ ns	$\tau_2 = 13$ ns	$\tau_3 = 348$ ns
$A_1 \tau_1 = 1.0$	$A_2 \tau_2 = 0.84$	$A_3 \tau_3 = 8.0$

(the products, $A_i \tau_i$ are normalized to $A_1 \tau_1 = 1$)

The two fast components provide the signal of interest discussed above. The slow component contains about four times as much charge (light) as the two fast components together. The contribution of the slow component to the pileup is negligible, particularly after pulse shaping, which removes the tail. This follows from evaluation of the pileup integral³.

The signal processing for all calorimetry techniques discussed here will have to be with a bipolar weighting function with area balance. Technically, this can be done in a number of ways: pulse shaping circuits, weighting of multiple samples, and sometimes bipolar weighting is disguised as "unipolar shaping with baseline subtraction".

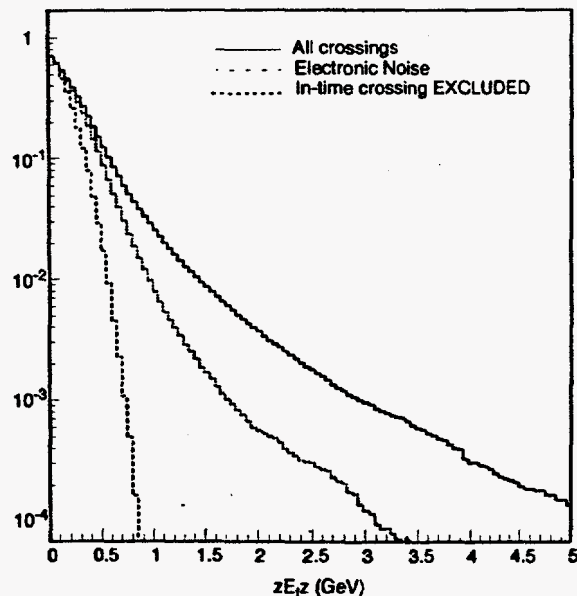


Fig. 2. Noise and pileup for 3 x 3 towers (0.025 x 0.025). Probability to get more than E_1^{\min} for a pileup of 20 superimposed min bias events with and without pileup from the considered bunch crossing⁶. Peaking time after shaping is ~ 45 ns.

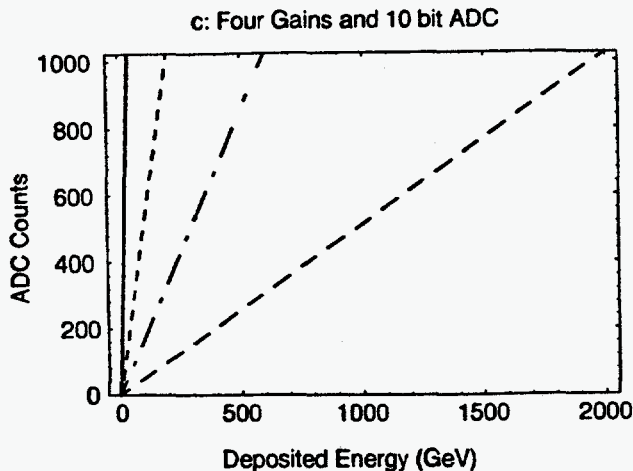
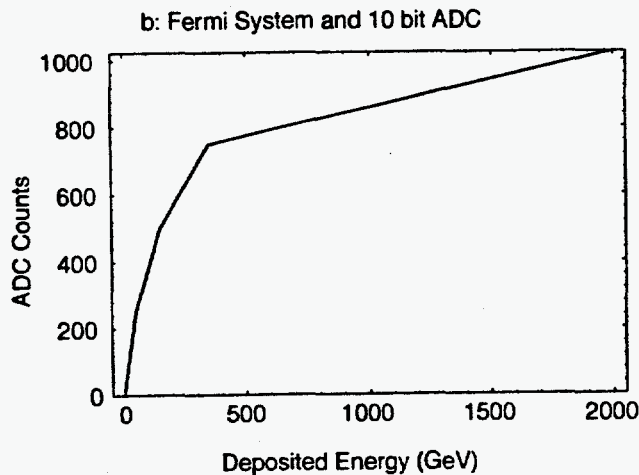
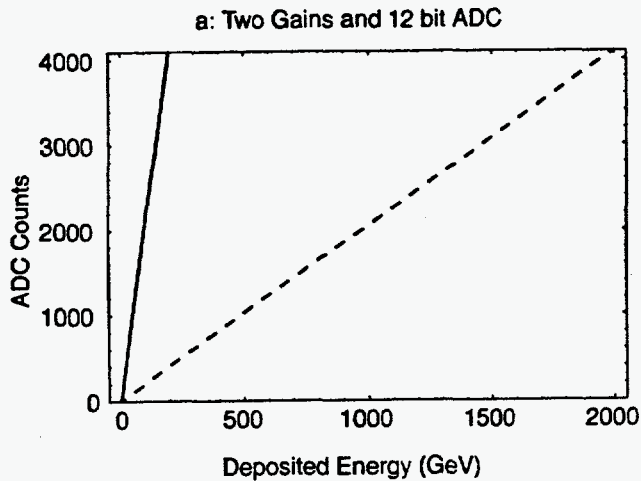


Fig. 3. ADC counts vs. energy for:
 a) two signal channels with high and low gain;
 b) FERMI scheme⁸ with dynamic range compression single channel in four segments;
 c) "four gain" scheme as in Fig. 5.

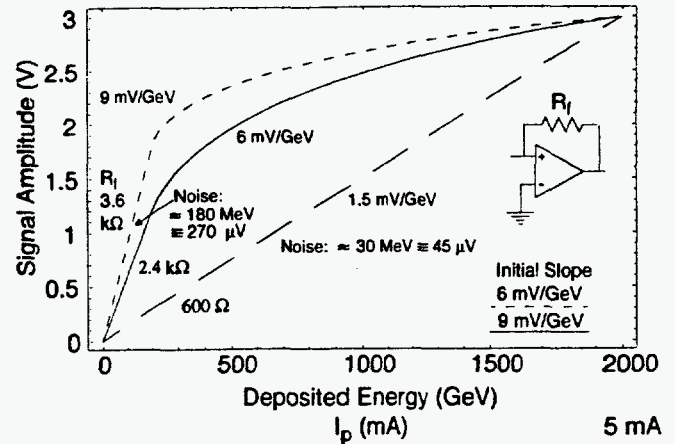


Fig. 4. Dynamic range compression in the preamplifier. The transimpedance (feedback resistance) defines the gain for small signals.

How short should the pulse shaping be to reduce pileup? Due to the bunching of particles at LHC in a short time interval (~ 1 ns) every 25 ns, most of the pileup at high luminosities ($\sim 10^{34}$ cm⁻² s⁻¹) arises from an average of ~ 20 events in one bunch crossing. This is illustrated in Fig. 3, a simulation for the LAr accordion EM calorimeter, in 3×3 towers ($0.075 \times 0.075 = \Delta\phi \times \Delta\eta$), after shaping with $t_m = 25$ ns, resulting in an output waveform with a peaking time of ≈ 45 ns as in Fig. 1(c). Thus, the benefit of shaping shorter than this diminishes. With crystals, the output pulse will be even shorter than with LAr for equal t_m , since it takes ~ 20 ns to collect 90% of the light from the fast components.

4. DYNAMIC RANGE AND COHERENT NOISE

The large dynamic range means that the random electronic noise in a single channel has to be low. For high resolution energy measurements, the signals from a number of channels have to be added up. It may take $3 \times 7 = 21$ towers ($\Delta\eta \times \Delta\phi = 0.025 \times 0.025$ each) to contain an EM shower in the magnetic field. With fine segmentation and subdivision in depth, the energy sum may require between 32 and 64 channels. The coherent noise from electromagnetic interference (EMI) increases linearly with the number of channels N (and not with the square root of N as for random noise). The interference noise can be expected to be coherent over localized regions, and on the readout cards where the channels forming energy sums are located. An illustration of the problem is given by looking at the signal levels (e.g., at the output of a preamplifier):

Max. signal:	2 TeV	2.5 V
Random noise/channel:	20 MeV	25 μ V
Sum of 64 channels: ($\propto N^{1/2}$)	160 MeV	200 μ V
Condition for coherent noise in the sum:		<64 μ V
Condition for coherent noise in one channel:		<1 μ V
Required attenuation of EMI (e.g., from digital transients):		$\geq 10^6$

already in the range of several volts, and the gain of subsequent stages is low, as it needs only to compensate for attenuation in the pulse shaping circuits. In a second stage amplifier (pulse shaper), it takes some effort to achieve a noise level of $\sim 2 \text{ nV/Hz}^{1/2}$. In $\sim 10 \text{ MHz}$ bandwidth of the pulse shaper, this results in $\sim 6 \text{ } \mu\text{V rms}$, which is only marginally low enough compared to the preamplifier noise of $25 \text{ } \mu\text{V}$ (in the table above). The noise generated between the shaper and the sampling circuit may be even more difficult to control. The bandwidth is greater, up to $\sim 100 \text{ MHz}$. The noise may also be higher than in the input of the second stage. With $5 \text{ nV/Hz}^{1/2}$ (which is not considered high for various commercial components), this would result in $\sim 50 \text{ } \mu\text{V}$, exceeding the preamplifier noise.

5. DYNAMIC RANGE AND READOUT SCHEMES

The interference noise may take different paths in the system, the worst is, directly into the detector electrode and the preamplifier input. While the random noise from the input transistors can be analyzed, predicted and measured with sufficient precision, the interference noise becomes apparent most often only when the system is assembled. Clearly it is a problem deserving early attention in the design.

In the readout chain, the limits to the maximum dynamic range appear in two ways: well defined specifications of performance, and less apparent deterioration in performance which requires extensive testing. In the first category is the nominal number of bits and the sampling frequency of an ADC. In the second is detailed nonlinearity of the ADC as a function of speed and on "effective number of bits", and any noise that is larger than a small fraction of the least significant bit. (Any noise added in the ADC has to be smaller than the noise of the preamplifier arriving to the ADC.) The dynamic range of an analog memory, with a switched capacitor array, is limited by various fine effects

The next noise problem, caused by the large dynamic range, is the *second and latter stage random noise*. This arises because the maximum signal from the preamplifier is

GAIN	50	10	3	1
ENERGY	30 GeV	150 GeV	450 GeV	1.5 TeV

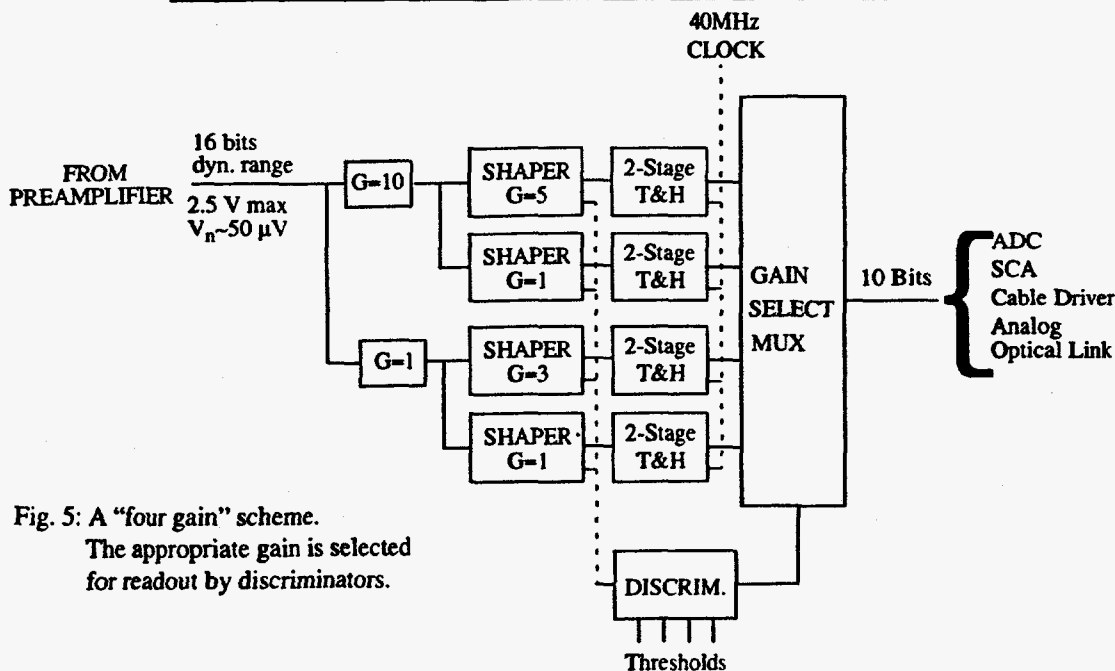


Fig. 5: A "four gain" scheme. The appropriate gain is selected for readout by discriminators.

which require great care in the design and in the testing in order to reach 12 to 13 bits⁹.

Since the dynamic range neither of analog memories nor of ADCs is sufficient, a number of readout schemes are being considered^{7,8,9}, with several linear ranges or with a single range and nonlinear dynamic range compression. These schemes are illustrated in terms of ADC counts vs energy (in one channel) in Fig. 3. In each case, the number of bits was chosen so as to make the quantization errors negligible compared to energy resolution. Schemes with two or more gain channels would require more analog memories and/or ADCs. An approach, where the most appropriate gain channel (out of four) would be selected, as illustrated

Preamplification is one link in thin Fig. 5, is being explored¹⁰. The readout chain which has the large dynamic range required. However, an approach to contain the full dynamic range in one channel for the whole readout chain, is by dynamic range compression in the preamplifier, or in a stage after the preamplifier. This is illustrated in Fig. 4. The response would be linear to a fairly high energy (e.g., ~ 250 GeV for an electron, ~ 150 GeV in one channel, as shown in the figure), and the top decade would be compressed. This raises the gain for small signals, makes the noise from latter stages negligible, and makes the transmission of signals by a cable possible. In all these schemes, the signals will be recorded by multiple sampling^{9,11,12,13}.

6. CONCLUDING REMARKS

Bunch crossing identification (BCID) has to be performed on signals formed by summation of signals from towers (and all sections in depth) comprising a trigger tower. This can be done by analog circuits and discriminators¹⁴, or by processing of the digitized trigger signal¹⁵. BCID has to be performed also on individual towers, at very low energies (a few hundred MeV) when checking for lepton isolation. All calorimeter techniques discussed here have good timing resolution to make this possible. A criterion for choosing the method for BCID on Level 1 trigger signals is the shortest latency.

Power dissipation on the detector. The design planning for both CMS and ATLAS is based on the assumption that signal shaping, analog or digital memory, and analog-to-digital conversion and/or multiplexing will be located on the calorimeter in order to avoid a large number of copper cables. Power estimates for this electronics are in the 0.5 - 1 W/channel range. With ~ 10⁵ channels (in the barrel alone), the total power of 50-100 kW, has to be brought to the detector as "clean power" (no switching power supplies?), and taken away as heat.

Reliability. The access to the electronics on the detector will be very limited and infrequent. This would tend to rule

out "quick fixes" and upgrades, and it would be best to design for reliability of operation over 5-10 years.

Acknowledgements

I would like to thank W. Cleland, S. Rescia, M. Seman, and C. Woody for help in preparation of the material for this presentation. Much valuable information was provided by P. Denes, J. Elias, and J. Pilcher.

References

1. V. Radeka, *Ann. Rev. Nucl. Sci.* 1988. 38:217.
2. C. de La Taille, "Electronic Noise in LAr Calorimetry", RD3 Note 45, LAL (May 1993).
J. Pascual, J. Teiger, ATLAS Note, CAL-NO-068, Nov. 1994.
3. V. Radeka, S. Rescia, *Nucl. Instr. and Meth.* A265 (1988) 228.
4. D. Camin et al., "Cryogenic Front-End Electronics in III-V Technology for Liquid Argon Calorimetry", *These Proceedings*, p. 257.
5. C. Woody, private communication.
6. I. Wingerter-Seez, ATLAS Note, LARG-NO-18, Apr. 1995.
7. G. Viertel, "Development of the Readout Electronics for the CMS Electromagnetic Calorimeter", *these Proceedings*, p. 278.
8. B. Lofstedt, "FERMI: a Digital Front End and Readout Microsystem for High Resolution Calorimetry", *these Proceedings*, p. 283.
9. J. Parsons, "Readout Electronics for the ATLAS LAr Calorimeter", *these Proceedings*, p. 265.
10. R. L. Chase, J. Parsons, W. Sippach, private communication.
11. W. E. Cleland, E. G. Stern, *Nucl. Instr. and Meth.:* A338 (1994) 467.
12. O. Benary et al., *Nucl. Instr. and Meth.* A349 (1994) 367.
13. O. Benary et al., *Nucl. Instr. and Meth.* A344 (1994) 363.
14. O. Benary et al., *Nucl. Instr. and Meth.* A332 (1993) 78.
15. I. Brawn, "Bunch-Crossing Identification for the ATLAS first-level Calorimeter Trigger", *these Proceedings*, p. 294.